Proceedings of the 10th Int. Symp. on Electromagnetic Compatibility, EMC Europe 2011, York, UK, pp. 351-356, September 26-30, 2011.

A Computation of the High-Frequency Per-Unit-Length Resistance Matrix of a Multiconductor Interconnection

Frédéric Broydé and Evelyne Clavelier
Tekcem
Maule, France
e-mail: fredbroyde@tekcem.com, eclavelier@tekcem.com

***Abstract* — Assuming the applicability of multiconductor transmission line (MTL) theory, we establish a relationship between the high-frequency (h.f.) current distribution in a multiconductor interconnection and the electrostatic charge distribution in a lossless interconnection without dielectrics. This result is used to obtain the h.f. per-unit-length resistance matrix at a low computational cost.**

I. Introduction

We consider a uniform multiconductor interconnection having n transmission conductors (TCs) and a reference conductor (ground), for instance used for signal transmission in a parallel link. A possible cross-section of such an $(n + 1)$-conductor interconnection is shown in Fig. 1, in the special case of a simple multiconductor microstrip structure. We want to describe the high-frequency (h.f.) current distribution in the cross-section of this "interconnection 1" and to use this result to compute its h.f. per-unit-length (p.u.l.) resistance matrix. In this paper, *h.f. current distribution* refers to the current distribution at frequencies for which the skin effect (current crowding near the surface of the conductors), the edge effect (current crowding near edges of the conductors) and the proximity effect (interaction of the current distributions in distinct nearby conductors) are fully developed.

In the case of a two-conductor interconnection ($n = 1$), the detailed current distribution is usually computed as the solution of equations involving the longitudinal electric field [1]. However, a different and older technique, which only applies in the quasi-TEM approximation, can be used to determine the h.f. current distribution at a low computational cost. It is based on the fact that the h.f. current distribution is the product of a constant and the charge distribution in the corresponding electrostatic problem [2]. In this paper, we carefully generalize this approach to the case $n \geq 2$. We do not take into account characteristics which might occur but are not necessarily present, such as inhomogeneous (e.g. plated) conductors [3, § III.B] or conductor roughness [4, § 5.3].

We define an "interconnection 2" as identical to the interconnection 1, except that, in the interconnection 2, the dielectrics are replaced with vacuum and the conductors are replaced with ideal conductors having the same geometry. In Section II, we review the propagation in the interconnection 2. In Sections III and IV, we establish general properties of the current and charge distributions in the interconnections 1 and 2. In Sections V and VI, these results are used to derive the h.f. current distribution and the h.f. p.u.l. resistance matrix of the interconnection 1. Examples are given in the Sections V and VII.

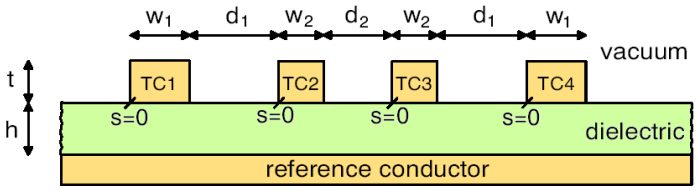

Fig. 1. Cross-section of a multiconductor microstrip interconnection comprising $n = 4$ transmission conductors (TCs) and a reference or ground conductor (GC). The arc length on the perimeter of each TC, denoted by s, is explained and used in Section V.

II. Lossless Interconnection Without Dielectrics

In the interconnection 2 defined in the introduction, we only consider the propagation of TEM waves along the z axis, which takes place at the velocity of light in vacuum, denoted by c_0. The most general frequency domain electric field solution is given by [5, § 9.1] [6, § 3.1]

$$\mathbf{E} = \mathbf{E}_A(x,y)\,e^{-j\frac{\omega}{c_0}z} + \mathbf{E}_B(x,y)\,e^{+j\frac{\omega}{c_0}z} \qquad (1)$$

where ω is the radian frequency, $\mathbf{E}_A(x, y)$ is a transverse electric field applicable to a wave propagating in the direction of increasing z, and $\mathbf{E}_B(x, y)$ is a transverse electric field applicable to a wave propagating in the direction of decreasing z. The two-dimensional fields $\mathbf{E}_A(x, y)$ and $\mathbf{E}_B(x, y)$ are related to the two-dimensional gradients of the potential functions $\psi_A(x, y)$ and $\psi_B(x, y)$, by $\mathbf{E}_A(x, y) = -\nabla_T \psi_A(x, y)$ and $\mathbf{E}_B(x, y) = -\nabla_T \psi_B(x, y)$, where ∇_T denotes the transverse part of the vector operator ∇. The magnetic field is given by

$$\mathbf{H} = \frac{1}{\eta_0}\mathbf{e}_z \times \left(\mathbf{E}_A(x,y)\,e^{-j\frac{\omega}{c_0}z} - \mathbf{E}_B(x,y)\,e^{+j\frac{\omega}{c_0}z} \right) \qquad (2)$$

where $\mathbf{e}_z$ denotes the unit vector of the z axis and η_0 is the intrinsic impedance of free-space. The equations (1) and (2) are direct consequences of Maxwell's equations.

$\psi_A(x, y)$ is the solution of Laplace's equation $\nabla_T{}^2 \psi_A(x, y) = 0$ for the Dirichlet boundary conditions defined by a column-vector $\mathbf{V}_A$ of voltages $V_{A\,1}, \ldots, V_{A\,n}$ between each TC and the ground conductor (GC); and $\psi_B(x, y)$ is the solution of Laplace's equation $\nabla_T{}^2 \psi_B(x, y) = 0$ for the Dirichlet boundary conditions defined by a column-vector $\mathbf{V}_B$ of voltages $V_{B\,1}, \ldots, V_{B\,n}$ between each TC and the GC. The vectors $\mathbf{V}_A$ and $\mathbf{V}_B$ are determined by the devices at the ends of the interconnection.

By (1) we see that $\mathbf{E}(x, y, z) = -\nabla_T \psi(x, y, z)$ where

$$\psi(x,y,z) = \psi_A(x,y)\, e^{-j\frac{\omega}{c_0}z} + \psi_B(x,y)\, e^{+j\frac{\omega}{c_0}z} \tag{3}$$

is the solution of Laplace's equation ${\nabla_T}^2 \psi(x, y, z) = 0$ for the Dirichlet boundary conditions defined by the column-vector $\mathbf{V}(z)$ of the voltages between each TC and the GC, given by

$$\mathbf{V}(z) = \mathbf{V}_A\, e^{-j\frac{\omega}{c_0}z} + \mathbf{V}_B\, e^{+j\frac{\omega}{c_0}z} \tag{4}$$

In the interconnection 2, at the boundary of the conductors, the surface charge density is given by

$$\rho_S = \varepsilon_0\, \mathbf{n} \cdot \left[\mathbf{E}_A(x,y)\, e^{-j\frac{\omega}{c_0}z} + \mathbf{E}_B(x,y)\, e^{+j\frac{\omega}{c_0}z} \right] \tag{5}$$

where ε_0 is the permittivity of vacuum and where $\mathbf{n}$ is the unit vector normal to the boundary drawn from the conductor to vacuum. The surface current density being axial (i.e. parallel to $\mathbf{e}_z$), the axial component of the surface current density on the surface of the conductors is given by

$$j_S = \mathbf{e}_z \cdot \left[\mathbf{n} \times \mathbf{H}(x,y,z) \right] \tag{6}$$

Using (2), we get

$$j_S = \frac{\mathbf{n}}{\eta_0} \cdot \left[\mathbf{E}_A(x,y)\, e^{-j\frac{\omega}{c_0}z} - \mathbf{E}_B(x,y)\, e^{+j\frac{\omega}{c_0}z} \right] \tag{7}$$

For a wave propagating in a given direction and $\alpha \in \{1,..., n\}$, an integration of (5) and (7) over the boundary of the TC α in a cross-section of the interconnection gives

$$I_\alpha(z) = \frac{\pm 1}{\eta_0 \varepsilon_0} Q_\alpha(z) = \pm c_0\, Q_\alpha(z) \tag{8}$$

where I_α and Q_α are the current in the TC α and the p.u.l. charge on the TC α, respectively, where the + sign applies to a wave propagating in the direction of increasing z, and the opposite sign to the opposite direction. Thus, using the definition of the p.u.l. capacitance matrix of the interconnection 2, a real matrix of size $n \times n$ denoted by $\mathbf{C}_0$, we get

$$\mathbf{I}(z) = \pm c_0\, \mathbf{C}_0\, \mathbf{V}(z) \tag{9}$$

where the column-vector of the currents in the TCs is denoted by $\mathbf{I}(z)$. By (4) we get

$$\mathbf{I}(z) = \mathbf{Z}_C^{-1} \left(\mathbf{V}_A\, e^{-j\frac{\omega}{c_0}z} - \mathbf{V}_B\, e^{+j\frac{\omega}{c_0}z} \right) \tag{10}$$

where $\mathbf{Z}_C = (c_0\, \mathbf{C}_0)^{-1}$ is the characteristic impedance matrix of the multiconductor transmission line (MTL).

We could have obtained (4) and (10) using general formulas for $\mathbf{V}(z)$ and $\mathbf{I}(z)$ provided by MTL theory [7, § 4.3.2], applied to the special case of lossless and homogeneous interconnection [7, § 4.4.1]. The above derivation has the advantage of showing that (4) and (10) are exact, direct and straightforward consequences of Maxwell's equations applied to TEM waves, and it also provides (5) and (7) which will be needed later in the paper.

III. Surface Current Density

Let us consider a first configuration where, at a given abscissa $z = z_G$ in the interconnection 2, a column-vector of the currents on the conductors, denoted by $\mathbf{I}(z_G)$, is observed. On the boundary of the conductors, according to (7), we may write

$$j_S = \frac{\mathbf{n}}{\eta_0} \cdot \mathbf{E}_G(x,y) = -\frac{\mathbf{n}}{\eta_0} \cdot \nabla_T \psi_G(x,y) \tag{11}$$

where

$$\mathbf{E}_G(x,y) = \mathbf{E}_A(x,y)\, e^{-j\frac{\omega}{c_0}z_G} - \mathbf{E}_B(x,y)\, e^{+j\frac{\omega}{c_0}z_G} \tag{12}$$

and

$$\psi_G(x,y) = \psi_A(x,y)\, e^{-j\frac{\omega}{c_0}z_G} - \psi_B(x,y)\, e^{+j\frac{\omega}{c_0}z_G} \tag{13}$$

Here, $\psi_G(x, y)$ is the solution of Laplace's equation ${\nabla_T}^2 \psi_G(x, y) = 0$ for the Dirichlet boundary conditions defined by

$$\mathbf{V}_A\, e^{-j\frac{\omega}{c_0}z_G} - \mathbf{V}_B\, e^{+j\frac{\omega}{c_0}z_G} = \mathbf{Z}_C \mathbf{I}(z_G) \tag{14}$$

where we have used (10). Consequently, the surface current density j_S does not depend on the choice of $\mathbf{V}_A$ and $\mathbf{V}_B$ and is uniquely defined by $\mathbf{I}(z_G)$. Clearly, $\psi_G(x, y)$ is a linear function of $\mathbf{I}(z_G)$, but it is otherwise independent of z_G and of frequency. Consequently, at a given (x, y) on the boundary of the conductors at $z = z_G$. Using (11) we find that j_S is a linear function of $\mathbf{I}(z_G)$, which may be represented with the matrix $\mathbf{M}(x, y)$ such that

$$j_S(x,y,z_G) = \mathbf{M}(x,y)\, \mathbf{I}(z_G) \tag{15}$$

where $\mathbf{M}(x, y)$ is frequency-independent and has the dimensions of m^{-1}. Moreover, we observe that, if $\mathbf{I}(z_G)$ is a real vector, $\psi_G(x, y)$ is a real potential function because, in (14), $\mathbf{Z}_C$ is a real matrix. Thus, if $\mathbf{I}(z_G)$ is a real vector, (11) shows that j_S is real, so that $\mathbf{M}(x, y)$ is real.

For the interconnection 1, our reasoning does not apply because (7) and (10) are not necessarily satisfied. Let us assume that resistive losses are small, so that the currents essentially flow near the surface of the conductors and a surface current density j_S can be considered. No general formula can be used in place of (7) and (10). This is not surprising, since MTL theory is exactly compatible with Maxwell equations only in the case of an homogeneous medium surrounding perfect conductors: in the general case where the dielectrics surrounding the conductors is not homogeneous, the fundamental mode of propagation is not exactly TEM [6, § 3.1]. However, in the framework of MTL theory, at each abscissa z, the effects of $\mathbf{I}(z)$, such as the magnetic field and the resulting j_S given by (6), are assumed to be independent from the effects of $\mathbf{V}(z)$, such as the electric field, so that, for a given $\mathbf{I}(z)$, j_S is unaffected by the presence of dielectrics. Thus, we can state the following theorem.

Theorem on the surface current density. At a given abscissa $z = z_G$ of the interconnection 1, for small resistive losses (h.f. current distribution), the surface current density j_S on the boundary of the conductors is given by (15), where $\mathbf{M}(x, y)$ is a real $1 \times n$ matrix which neither depends on the abscissa nor on the frequency.

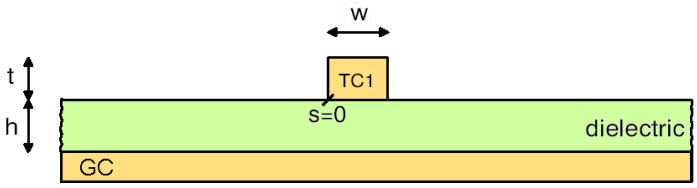

Fig. 2. Cross-section of a microstrip interconnection, showing the origin of the arc length on the perimeter of the TC, denoted by *s*.

IV. Surface Charge Density

Let us consider a second configuration where, at an abscissa $z = z_H$ in the interconnection 2, a column-vector of the p.u.l. charge density on the boundary of the conductors, denoted by $\mathbf{Q}(z_H)$, is observed. By charge conservation, we have

$$j\omega\,\mathbf{Q}(z_H) = -\left.\frac{d\,\mathbf{I}}{dz}\right|_{z_H} \tag{16}$$

Using (4) and (10), we get

$$\mathbf{Q}(z_H) = \frac{\mathbf{Z}_C^{-1}}{c_0}\left(\mathbf{V}_A\, e^{-j\frac{\omega}{c_0}z_H} + \mathbf{V}_B\, e^{+j\frac{\omega}{c_0}z_H}\right) = \frac{\mathbf{Z}_C^{-1}\mathbf{V}(z_H)}{c_0} \tag{17}$$

At $z = z_H$, on the boundary of the conductors, by (5) we have

$$\rho_S = \varepsilon_0\,\mathbf{n}\cdot\mathbf{E}_H = -\varepsilon_0\,\mathbf{n}\cdot\nabla_T\psi_H \tag{18}$$

where

$$\mathbf{E}_H(x,y) = \mathbf{E}_A(x,y)\,e^{-j\frac{\omega}{c_0}z_H} + \mathbf{E}_B(x,y)\,e^{+j\frac{\omega}{c_0}z_H} \tag{19}$$

and

$$\psi_H(x,y) = \psi_A(x,y)\,e^{-j\frac{\omega}{c_0}z_H} + \psi_B(x,y)\,e^{+j\frac{\omega}{c_0}z_H} \tag{20}$$

Here, $\psi_H(x, y)$ is the solution of Laplace's equation $\nabla_T{}^2\psi_H(x, y) = 0$ for the Dirichlet boundary conditions defined by

$$\mathbf{V}_A\, e^{-j\frac{\omega}{c_0}z_H} + \mathbf{V}_B\, e^{+j\frac{\omega}{c_0}z_H} = \mathbf{V}(z_H) = c_0\,\mathbf{Z}_C\mathbf{Q}(z_H) \tag{21}$$

where we have used (17). Thus, the surface charge density ρ_S is uniquely defined by $\mathbf{V}(z_H)$ or equivalently by $\mathbf{Q}(z_H)$. We see that $\psi_H(x, y)$ is a linear function of $\mathbf{Q}(z_H)$, but it is otherwise independent of z_H and of the frequency. Consequently, at a given (x, y) on the boundary of the conductors at $z = z_H$, ρ_S is a linear function of $\mathbf{Q}(z_H)$, which may be represented with the frequency-independent matrix $\mathbf{N}(x, y)$ such that

$$\rho_S(x,y,z_H) = \mathbf{N}(x,y)\,\mathbf{Q}(z_H) \tag{22}$$

where $\mathbf{N}(x, y)$ has the dimensions of m^{-1}. Additionally, we observe that, if $\mathbf{Q}(z_H)$ is a real vector, $\psi_H(x, y)$ and $\mathbf{V}(z_H)$ are real by (21) because $\mathbf{Z}_C$ is a real matrix. Thus, if $\mathbf{Q}(z_H)$ is real, (18) shows that ρ_S is real, so that $\mathbf{N}(x, y)$ is real and describes the electrostatic charge distribution. We have proved a second theorem.

Theorem on the surface charge density. At a given abscissa $z = z_H$ of the interconnection 2, the surface charge density ρ_S on the boundary of the conductors is given by (22), where $\mathbf{N}(x, y)$ is a real $1 \times n$ matrix which neither depends on the abscissa nor on the frequency, $\mathbf{N}(x, y)$ describing the electrostatic charge distribution.

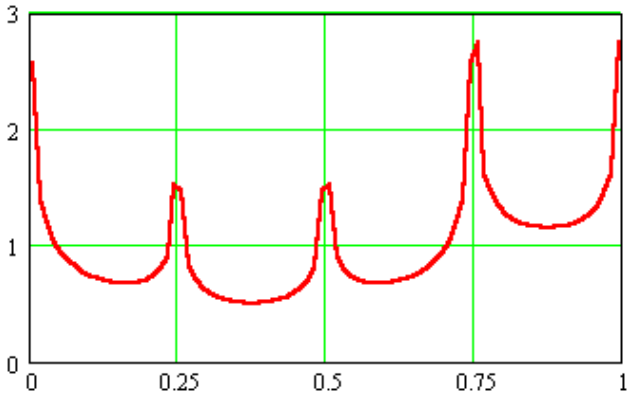

Fig. 3. For the interconnection shown in Fig. 2, surface current density on the TC (arbitrary unit) versus *s* when a current is injected in the TC.

V. High-Frequency Current Distribution

We now observe that $\psi_G(x, y)$ and $\psi_H(x, y)$ are the solutions of Laplace's equation for the Dirichlet boundary conditions defined by $\mathbf{Z}_C\ \mathbf{I}(z_G)$ and $c_0\ \mathbf{Z}_C\ \mathbf{Q}(z_H)$, respectively. Thus, for $\mathbf{I}(z_G) = c_0\ \mathbf{Q}(z_H)$ we have $\psi_G(x, y) = \psi_H(x, y)$, so that by (11) and (18) we have $\rho_S/\varepsilon_0 = \eta_0 j_S$. Consequently,

$$\mathbf{N}(x, y) = \mathbf{M}(x, y) \tag{23}$$

Thus, we obtain the following theorem.

Theorem on the connection of charge and current densities. For an MTL with small resistive losses (h.f. current distribution), at a given abscissa z, for a given $\mathbf{I}(z)$, the surface current density j_S at the surface of the conductors is the product of an arbitrary velocity v_D and the surface charge density at the surface of the conductors in a configuration where all dielectrics are replaced by vacuum and where $\mathbf{Q}(z) = \mathbf{I}(z)/v_D$.

Let us now see how this theorem can be used to easily determine the h.f. current distribution. The MTL model of the interconnection includes the h.f. p.u.l. external inductance matrix of the interconnection 1, denoted by $\mathbf{L}_0$. We show in the Appendix that this matrix is given by $\mathbf{L}_0 = \mu_0\ \varepsilon_0\ \mathbf{C}_0{}^{-1}$, where μ_0 is the permeability of vacuum and $\mathbf{C}_0$ was defined in Section II. In order to assess $\mathbf{C}_0$, the perimeter of each TC is usually divided in small strips. Let us use A to denote the set of the indices of the strips which form the boundaries of all TCs. The set A may be partitioned into mutually exclusive subsets A_1, ... A_n, where for any integer j such that $1 \le j \le n$, the subset A_j contains the indices of the strips of the TC number j. At the final stage of the computation of $\mathbf{C}_0$ by the method of moment using pulse expansion and point matching [7, § 3.3], a capacitance matrix $\mathcal{C}_0$ is computed, an entry $\mathcal{C}_{0\alpha\beta}$ of $\mathcal{C}_0$ being the p.u.l. charge of the strip number α when the voltage between the center of the strip number β and ground is 1 V, the voltage between the center of each other strip and ground being 0 V. The entry C_{0ij} of $\mathbf{C}_0$ is given by

$$C_{0ij} = \sum_{\alpha\in A_i}\sum_{\beta\in A_j}\mathcal{C}_{0\alpha\beta} \tag{24}$$

At this point, an estimate of $\mathbf{N}(x, y) = \mathbf{M}(x, y)$ is available, since,

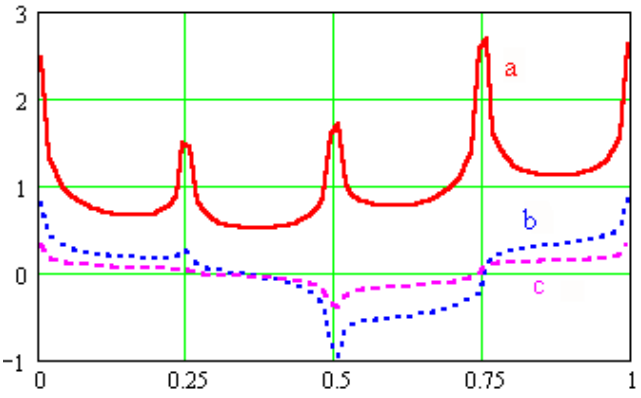

Fig. 4. For the interconnection shown in Fig. 1, surface current density (arbitrary unit) measured on TC 1, versus *s*, when a current is injected in the TC 1 (a), TC 2 (b) or TC 3 (c).

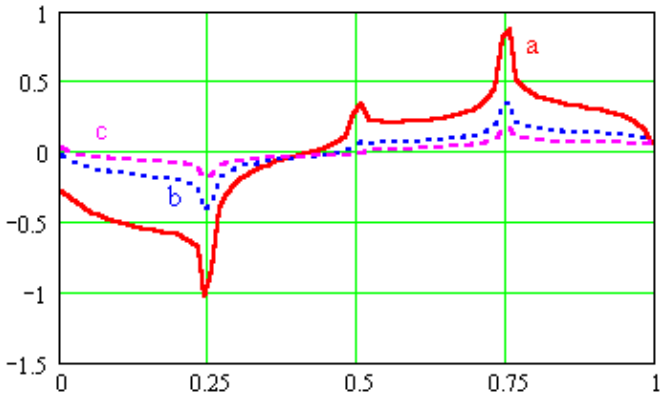

Fig. 5. For the interconnection shown in Fig. 1, surface current density (arbitrary unit) versus *s* when a current is injected in the TC 1: measured on TC 2 (a), TC 3 (b) and TC 4 (c).

at any point (X, Y) on the strip number α we have

$$\mathbf{N}(X,Y) \approx \frac{1}{w_\alpha} \sum_{j=1}^{n} \left(\sum_{\beta \in A_j} \mathcal{C}_{0\alpha\beta} \right) {}^t\mathbf{e}_j \mathbf{C}_0^{-1} \qquad (25)$$

where we use w_α to denote the width of the strip α, where ${}^t\mathbf{A}$ denotes the transpose of $\mathbf{A}$ and where $\mathbf{e}_j$ denotes the column-vector having n entries, said entries being zero except the j-th entry which is equal to 1.

Let us for instance consider the interconnection shown in Fig. 2, with $t = w = h = 50$ µm. On the TC, the normalized arc length along the perimeter of the cross section, denoted by s, increases clockwise, from the point $s = 0$, shown in Fig. 2, to $s = 1$. The Fig. 3 shows the h.f. current distributions on the TC when a current is injected into it, computed using (25) and 84 matching points. The edge effect, which causes current crowding near edges, is visible in Fig. 2, at $s = 0$, $s = 0.25$, $s = 0.5$, $s = 0.75$, and $s = 1$. The proximity effect increases the current on the bottom of the TC.

Let us now consider the interconnection shown in Fig. 1, with $t = w_1 = w_2 = h = d_1 = d_2 = 50$ µm. On a given TC, the normalized arc length is defined as in Fig. 2. The Fig. 4 and Fig. 5 show the h.f. current distributions on the TCs when a current is injected on a single TC, the other TCs being open circuited, computed using (25) and 336 matching points. The edge effect and the proximity effect are plain in Fig. 4 and Fig. 5. We see that the proximity effect causes eddy currents to be induced in all non-excited conductors. This phenomenon will contribute to the h.f. resistive losses. The Fig. 6 shows the h.f. current distributions in the GC when a current is injected on a single TC. These distributions are governed by the proximity effect. We observe that the different return current paths do not exactly have the same distribution, because of the interactions between the TCs. Also, the return current paths overlap, this effect creating a resistive coupling proportional to the common h.f. resistance.

VI. High-Frequency P.U.L. Resistance Matrix

Let us assume that we inject the currents of the column-vector $\mathbf{I}$ into the TCs. Let us use $i_S(\alpha, \mathbf{I})$ to denote the current flowing in the strip α. For any $j \in \{1,..., n\}$, we have

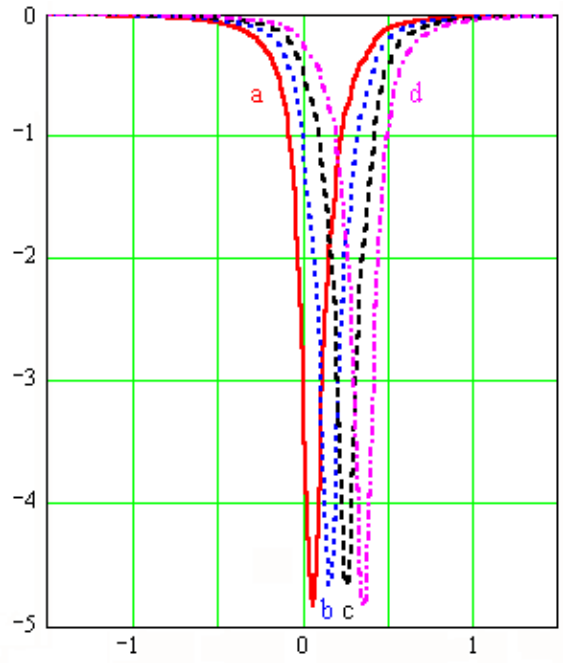

Fig. 6. Surface current density (arbitrary unit) on the reference conductor (GC), versus the abscissa in the cross-section in mm, when a current is injected in the TC 1 (a), TC 2 (b), TC 3 (c) or TC 4 (d).

$$\sum_{\alpha \in A_j} i_S(\alpha, \mathbf{I}) = [\mathbf{I}]_j \qquad (26)$$

where $[\mathbf{x}]_j$ is the j-th entry of the vector $\mathbf{x}$. At high frequencies, according to the theorem on the surface current density, we may define a real matrix $\mathbf{Q}_V$ having n columns such that, for any $\mathbf{I}$, the current flowing in the strip α is given by

$$i_S(\alpha, \mathbf{I}) = k [\mathbf{Q}_V \ \mathbf{I}]_\alpha \qquad (27)$$

where k is an arbitrary non-zero constant. Using (26), we get

$$i_S(\alpha, \mathbf{I}) = \sum_{j=1}^{n} \frac{Q_{V\alpha j} I_j}{\sum_{\beta \in A_j} Q_{V\beta j}} \qquad (28)$$

where the $Q_{V\,\alpha\,j}$ are the entries of $\mathbf{Q}_V$. Let us assume that the resistivity and the skin depth are the same in all TCs and denoted by ρ_{TC} and δ_{TC}, respectively. At sufficiently high frequencies, the thickness and width of each TC are each much greater than δ_{TC}. In this case, the surface current density being homogeneous over each strip, the p.u.l. power dissipated in the TCs is

$$P_{TC} = \frac{\rho_{TC}}{\delta_{TC}} \sum_{\alpha \in A} \frac{\left| i_S(\alpha, \mathbf{I}) \right|^2}{w_\alpha} \tag{29}$$

The h.f. p.u.l. resistance matrix of the TCs, denoted by $\mathbf{R}_{HFTC}$, is defined by $P_{TC} = \mathbf{I}^* \mathbf{R}_{HFTC} \mathbf{I}$, where $\mathbf{I}^*$ denotes the hermitian adjoint of $\mathbf{I}$. Using (28) and (29), we may easily show that

$$\mathbf{R}_{HFTC} = \frac{\rho_{TC}}{\delta_{TC}} \mathbf{K}_{TC} \tag{30}$$

where we refer to $\mathbf{K}_{TC}$ as the matrix of the equivalent inverse widths of the TCs, the entries of $\mathbf{K}_{TC}$ being given by

$$K_{TC\,i\,j} = \frac{1}{\left(\sum_{\beta \in A_i} Q_{V\,\beta\,i} \right) \left(\sum_{\beta \in A_j} Q_{V\,\beta\,j} \right)} \sum_{\alpha \in A} \frac{Q_{V\,\alpha i} Q_{V\,\alpha\,j}}{w_\alpha} \tag{31}$$

At this stage, the theorem on the connection of charge and current densities can be used to obtain $\mathbf{Q}_V$, since it tells us that we may define $Q_{V\,\alpha\,i}$ as the p.u.l. electrostatic charge on the strip α when the p.u.l charge of the TC number i is 1, the p.u.l. charge on each other TC being zero. In other words, we can use

$$Q_{V\,\alpha i} = \sum_{j=1}^{n} \left(\sum_{\beta \in A_j} \mathcal{C}_{0\alpha\beta} \right) {}^t\mathbf{e}_j \mathbf{C}_0^{-1} \mathbf{e}_i \tag{32}$$

A similar reasoning can be used to obtain the h.f. p.u.l. resistance matrix of the GC, denoted by $\mathbf{R}_{HFGC}$ and defined by $P_{GC} = \mathbf{I}^* \mathbf{R}_{HFGC} \mathbf{I}$, where P_{GC} is the p.u.l. power dissipated in the GC. Using ρ_{GC} and δ_{GC} to denote the resistivity and the skin depth of the GC, respectively, we find

$$\mathbf{R}_{HFGC} = \frac{\rho_{GC}}{\delta_{GC}} \mathbf{K}_{GC} \tag{33}$$

where we refer to $\mathbf{K}_{GC}$ as the matrix of the equivalent inverse widths of the GC, the entries of $\mathbf{K}_{GC}$ being given by

$$K_{GC\,i\,j} = \frac{\int_C \left\{ \mathbf{n} \cdot \mathbf{E}_i(\xi) \right\} \left\{ \mathbf{n} \cdot \mathbf{E}_j(\xi) \right\} d\xi}{\left(\int_C \mathbf{n} \cdot \mathbf{E}_i(\xi)\, d\xi \right) \left(\int_C \mathbf{n} \cdot \mathbf{E}_j(\xi)\, d\xi \right)} \tag{34}$$

where ξ is an arc length on the boundary of the GC and where $\mathbf{n} \cdot \mathbf{E}_i(\xi)$ is the electrostatic field component normal to the surface of the GC when the p.u.l. charge of each strip is given by (32), the integration path C extending over the boundary of the GC.

Finally, the h.f. resistance matrix of the interconnection, denoted by $\mathbf{R}_{HF}$, is given by

$$\mathbf{R}_{HF} = \mathbf{R}_{HFTC} + \mathbf{R}_{HFGC} = \frac{\rho_{TC}}{\delta_{TC}} \mathbf{K}_{TC} + \frac{\rho_{GC}}{\delta_{GC}} \mathbf{K}_{GC} \tag{35}$$

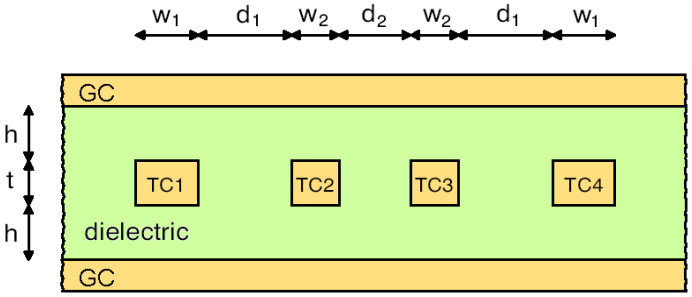

Fig. 7. Cross-section of a multiconductor stripline interconnection.

The conductors being reciprocal and passive, $\mathbf{K}_{TC}$ and $\mathbf{K}_{GC}$ are frequency-independent real positive semidefinite matrices [8, § 7.1]. Thus, any diagonal entry of $\mathbf{K}_{TC}$ or $\mathbf{K}_{GC}$ is non-negative.

VII. Examples

As a first example, we consider the microstrip interconnection used in Section V and depicted in Fig. 2, with $t = w = h = 50$ µm and a dielectric of relative permittivity $\varepsilon_r = 12.9$. This case was studied and discussed in [3, § III.D]. Using 84 matching points, we find that the p.u.l. external inductance, the p.u.l. capacitance, and K_{TC} and K_{GC} given by (31), (32) and (34) are

$$\begin{aligned} L_0 &= 317.5 \text{ nH/m} & C &= 236.3 \text{ pF/m} \\ K_{TC} &= 6176 \text{ m}^{-1} & K_{GC} &= 2392 \text{ m}^{-1} \end{aligned} \tag{36}$$

As a second example, we consider the multiconductor microstrip interconnection used in Section V and shown in Fig. 1, for which $t = w_1 = w_2 = h = d_1 = d_2 = 50$ µm, again with $\varepsilon_r = 12.9$. Using 336 matching points, we find that the p.u.l. external inductance matrix and the p.u.l. capacitance matrix are

$$\mathbf{L}_0 = \begin{pmatrix} 303.9 & 103.0 & 42.4 & 21.1 \\ 103.0 & 293.8 & 99.8 & 42.4 \\ 42.4 & 99.8 & 293.8 & 103.0 \\ 21.1 & 42.4 & 103.0 & 303.9 \end{pmatrix} \text{nH/m} \tag{37}$$

and

$$\mathbf{C} = \begin{pmatrix} 242.3 & -27.3 & -1.0 & -0.5 \\ -27.3 & 248.1 & -27.0 & -1.0 \\ -1.0 & -27.0 & 248.1 & -27.3 \\ -0.5 & -1.0 & -27.3 & 242.3 \end{pmatrix} \text{pF/m} \tag{38}$$

$\mathbf{K}_{TC}$ and $\mathbf{K}_{GC}$ given by (31), (32) and (34) are:

$$\mathbf{K}_{TC} = \begin{pmatrix} 6961 & 806 & 88 & 0 \\ 806 & 7466 & 985 & 88 \\ 88 & 985 & 7466 & 806 \\ 0 & 88 & 806 & 6961 \end{pmatrix} \text{m}^{-1} \tag{39}$$

and

$$\mathbf{K}_{GC} = \begin{pmatrix} 2238 & 1622 & 951 & 563 \\ 1622 & 2157 & 1582 & 951 \\ 951 & 1582 & 2157 & 1622 \\ 563 & 951 & 1622 & 2238 \end{pmatrix} \text{m}^{-1} \tag{40}$$

As a third example, we consider the multiconductor stripline interconnection depicted in Fig. 7, with the same parameter values and computation technique as the second example. We find

$$\mathbf{L}_0 = \begin{pmatrix} 229.5 & 47.6 & 10.0 & 2.1 \\ 47.6 & 224.4 & 46.6 & 10.0 \\ 10.0 & 46.6 & 224.4 & 47.6 \\ 2.1 & 10.0 & 47.6 & 229.5 \end{pmatrix} \text{nH/m} \tag{41}$$

$$\mathbf{C} = \begin{pmatrix} 654.3 & -138.8 & -0.2 & -0.0 \\ -138.8 & 697.9 & -138.8 & -0.2 \\ -0.2 & -138.8 & 697.9 & -138.8 \\ -0.0 & -0.2 & -138.8 & 654.3 \end{pmatrix} \text{pF/m} \tag{42}$$

$$\mathbf{K}_{TC} = \begin{pmatrix} 6101 & 163 & -186 & -91 \\ 163 & 6411 & 246 & -186 \\ -186 & 246 & 6411 & 163 \\ -91 & -186 & 163 & 6101 \end{pmatrix} \text{m}^{-1} \tag{43}$$

and

$$\mathbf{K}_{GC} = \begin{pmatrix} 1992 & 1099 & 378 & 113 \\ 1099 & 1882 & 1064 & 378 \\ 378 & 1064 & 1882 & 1099 \\ 113 & 378 & 1099 & 1992 \end{pmatrix} \text{m}^{-1} \tag{44}$$

As expected, each diagonal entries of $\mathbf{C}$ given by (42) is greater than the corresponding entries given by (38) and each diagonal entry of $\mathbf{L}_0$, $\mathbf{K}_{TC}$ and $\mathbf{K}_{GC}$ given by (41), (43) and (44) is less than the corresponding entry given by (37), (39) or (41). More importantly, this third example shows that a non-diagonal entry of $\mathbf{K}_{TC}$ is not always positive. We have checked that, for the second and third examples, $\mathbf{K}_{TC}$ and $\mathbf{K}_{GC}$ are positive semidefinite.

We have computed $\mathbf{K}_{TC}$ and $\mathbf{K}_{GC}$ in many different configurations. We always found that $\mathbf{K}_{TC}$ is strictly diagonally dominant [8, § 6.1.9], and that $\mathbf{K}_{GC}$ is nonnegative [8, § 8.1].

VIII. Conclusion

We have used the assumptions of TEM propagation in the interconnection 2 and of the applicability of the MTL model to the interconnection 1 to obtain some properties of the current and charge distributions, which include a relationship between the h.f. current distribution in the interconnection 1 and the electrostatic charge distribution in the interconnection 2. This relationship can be used to easily determine a h.f. current distribution which takes into account the crowding of currents at the edges of each conductor (edge effect), and the interactions between the currents flowing in different conductors (proximity effect).

In the case where the TCs have the same homogeneous resistivity, it is convenient to compute the frequency-independent $\mathbf{K}_{TC}$ and $\mathbf{K}_{GC}$ to obtain the frequency-dependent $\mathbf{R}_{HFTC}$ and $\mathbf{R}_{HFGC}$ at any frequency where the h.f. approximation applies. We have provided formula for evaluating $\mathbf{K}_{TC}$ and $\mathbf{K}_{GC}$ at a low computational cost after the computation of $\mathbf{L}_0$.

This work may be used to define an analytical and physically reasonable model for the p.u.l. internal impedance matrix at any frequency where the quasi-TEM assumption applies [9].

Appendix: A Note on MTL Theory

Using (4) and (10), we get

$$\frac{d\,\mathbf{V}}{dz} = \frac{d}{dz}\left(\mathbf{V}_A\, e^{-j\frac{\omega}{c_0}z} + \mathbf{V}_B\, e^{+j\frac{\omega}{c_0}z}\right) = -j\omega\,\frac{\mathbf{C}_0^{-1}}{c_0^2}\mathbf{I} \tag{45}$$

and

$$\frac{d\,\mathbf{I}}{dz} = c_0\,\mathbf{C}_0\frac{d}{dz}\left(\mathbf{V}_A\, e^{-j\frac{\omega}{c_0}z} - \mathbf{V}_B\, e^{+j\frac{\omega}{c_0}z}\right) = -j\omega\,\mathbf{C}_0\mathbf{V} \tag{46}$$

Assuming only TEM propagation, we have proved the telegrapher's equations for the interconnection 2, given by

$$\begin{cases} \dfrac{d\,\mathbf{V}}{dz} = -j\omega\,\mathbf{L}_0\,\mathbf{I} \\ \dfrac{d\,\mathbf{I}}{dz} = -j\omega\,\mathbf{C}_0\mathbf{V} \end{cases} \tag{47}$$

where $\mathbf{L}_0$ is the p.u.l. inductance matrix of the interconnection 2, given by

$$\mathbf{L}_0 = \frac{1}{c_0^2}\mathbf{C}_0^{-1} = \mu_0\varepsilon_0\,\mathbf{C}_0^{-1} \tag{48}$$

$\mathbf{L}_0$ is also the h.f. p.u.l. external inductance matrix of the interconnection 1. Most authors use (48) without proof [7, § 2.4] [10, § 6.2.6.1]. We are aware of only two proofs [11, § IV.3] [12, Appendix], but they are much more complex than the present one.

References

[1] A. Cangellaris, "A Note on the calculation of the current distribution in lossy microstrip structures", *IEEE Microwave Guided Wave Lett.*, Vol. 1, No. 4, April 1991, pp. 81-83.

[2] W. Thomson, "On Alternate Currents in Parallel Conductors of Homogeneous or Heterogeneous Substance", in *Mathematical and Physical Papers*, Vol. V, Cambridge University Press, 1911, pp. 489-495.

[3] T. Demeester, D. De Zutter, "Internal Impedance of Composite Conductors with Arbitrary Cross Section", *IEEE Trans. Electromagnetic Compatibility*, vol. 51, No. 1, February 2009, pp. 101-107.

[4] S.H. Hall, H.L. Heck, *Advanced Signal Integrity for High-Speed Digital Designs*, John Wiley & Sons, 2009.

[5] C.T.A. Johnk, *Engineering Electromagnetic Fields and Waves*, John Wiley & Sons, 1975.

[6] R.E. Collin, *Field Theory of Guided Waves*, 2nd ed., IEEE Press, 1991.

[7] C.R. Paul, *Analysis of Multiconductor Transmission Lines*, John Wiley & Sons, 1994.

[8] R.A. Horn, C.R. Johnson, *Matrix analysis*, Cambridge University Press, 1985.

[9] F. Broydé, E. Clavelier, "A Passive Analytical Per-Unit-Length Internal Impedance Matrix Model for Multiconductor Interconnections", *Proc. 2011 IEEE Int. Symp. on Electromagnetic Compatibility, EMC 2011*, Aug. 2011.

[10] F.M. Tesche, M.V. Ianoz, T. Karlsson, *EMC Analysis Methods and Computational Models*, New York, N.Y.: John Wiley & Sons, 1997.

[11] L.A. Pipes, "Steady-State Analysis of Multiconductor Transmission Lines", *Journal of Applied Physics*, vol. 12, November 1941, pp. 782-799.

[12] C. Wei, R.F. Harrington, J.R. Mautz, T.K. Sarkar, "Multiconductor Transmission Lines in Multilayered Dielectric Media", *IEEE Trans. on Microwave Theory Tech.*, vol. 32, No. 4, April 1984, pp. 439-450.